Array Phase Shifters: Theory and Technology

Robert R. Romanofsky
Glenn Research Center, Cleveland, Ohio

NASA STI Program . . . in Profile

Since its founding, NASA has been dedicated to the advancement of aeronautics and space science. The NASA Scientific and Technical Information (STI) program plays a key part in helping NASA maintain this important role.

The NASA STI Program operates under the auspices of the Agency Chief Information Officer. It collects, organizes, provides for archiving, and disseminates NASA's STI. The NASA STI program provides access to the NASA Aeronautics and Space Database and its public interface, the NASA Technical Reports Server, thus providing one of the largest collections of aeronautical and space science STI in the world. Results are published in both non-NASA channels and by NASA in the NASA STI Report Series, which includes the following report types:

- TECHNICAL PUBLICATION. Reports of completed research or a major significant phase of research that present the results of NASA programs and include extensive data or theoretical analysis. Includes compilations of significant scientific and technical data and information deemed to be of continuing reference value. NASA counterpart of peer-reviewed formal professional papers but has less stringent limitations on manuscript length and extent of graphic presentations.

- TECHNICAL MEMORANDUM. Scientific and technical findings that are preliminary or of specialized interest, e.g., quick release reports, working papers, and bibliographies that contain minimal annotation. Does not contain extensive analysis.

- CONTRACTOR REPORT. Scientific and technical findings by NASA-sponsored contractors and grantees.

- CONFERENCE PUBLICATION. Collected papers from scientific and technical conferences, symposia, seminars, or other meetings sponsored or cosponsored by NASA.

- SPECIAL PUBLICATION. Scientific, technical, or historical information from NASA programs, projects, and missions, often concerned with subjects having substantial public interest.

- TECHNICAL TRANSLATION. English-language translations of foreign scientific and technical material pertinent to NASA's mission.

Specialized services also include creating custom thesauri, building customized databases, organizing and publishing research results.

For more information about the NASA STI program, see the following:

- Access the NASA STI program home page at *http://www.sti.nasa.gov*

- E-mail your question via the Internet to *help@sti.nasa.gov*

- Fax your question to the NASA STI Help Desk at 301–621–0134

- Telephone the NASA STI Help Desk at 301–621–0390

- Write to:
  NASA Center for AeroSpace Information (CASI)
  7115 Standard Drive
  Hanover, MD 21076–1320

Array Phase Shifters: Theory and Technology

Robert R. Romanofsky
Glenn Research Center, Cleveland, Ohio

Contents

Array Phase Shifters:
Theory and Technology

Robert R. Romanofsky
National Aeronautics and Space Administration
Glenn Research Center
Cleveland, Ohio 44135

Introduction

While there are a myriad of applications for microwave phase shifters in instrumentation and metrology, power combining, amplifier linearization, and so on, the most prevalent use is in scanning phased-array antennas. And while this market continues to be dominated by military radar and tracking platforms, many commercial applications have emerged in the past decade or so. These new and potential applications span low-Earth-orbit (LEO) communications satellite constellations and collision warning radar, an aspect of the Intelligent Vehicle Highway System or Automated Highway System. In any case, the phase shifters represent a considerable portion of the overall antenna cost, with some estimates approaching 40 percent for receive arrays. Ferrite phase shifters continue to be the workhorse in military-phased arrays, and while there have been advances in thin film ferrite devices, the review of this device technology in the previous edition of this book is still highly relevant. This chapter will focus on three types of phase shifters that have matured in the past decade: GaAs MESFET monolithic microwave integrated circuit (MMIC), micro-electromechanical systems (MEMS), and thin film ferroelectric-based devices. A brief review of some novel devices including thin film ferrite phase shifters and superconducting switches for phase shifter applications will be provided. Finally, the effects of modulo 2π phase shift limitations, phase errors, and transient response on bit error rate degradation will be considered.

Applications

Military applications emphasize ground based systems for early warning radar, missile defense, and space surveillance. Most of the systems employ ferrite phase shifter technology, but several examples of GaAs MMIC based arrays exist. Space applications, including civilian space applications, include synthetic aperture radar and satellite communications. Another burgeoning commercial application is collision warning and collision avoidance radar for the Intelligent Vehicle Highway System.

Military Phased Array Antennas

Table 1 summarizes some of the military phased array radar systems (refs. 1 and 2). Note that many of the arrays developed during the last three decades had production runs of over 50 and that even one radar system can necessitate a very large number of phase shifters.

The last two systems use MMIC modules. The Theater High Altitude Area Defense (THAAD) ground-based radar required over 60,000 MMIC phase shifter chips. The program demonstrated a per-module cost of about $1,000. The Counter Battery Radar (COBRA) artillery and mortar weapon-locating system required more than 8,000 MMIC modules.

TABLE 1.—PHASED ARRAY SYSTEM EXAMPLES
(Reprinted with permission from *Microwave Journal*, vol. 40, no. 5, May 1997, pp. 288–294)

System	Frequency band	Number manufactured	Phase shifters per array	Elements manufactured	Manufacturer
AN/TPN-25	X	18	824	14,850	Raytheon
AN/GPN-22	X	60	443	26,580	Raytheon
Cobra Dane	L	1	34,769	34,769	Raytheon
Pave Paws	UHF	4	2,667	21,416	Raytheon
BMEWS	UHF	2	3,584	17,920	Raytheon
Cobra Judy	-	1	12,288	12,288	Raytheon
Patriot	C	173	5,000	865,000	Raytheon
AEGIS/SPY-1	S	234	4,000	936,000	Raytheon
B-1	X	100	1,526	152,600	Northrup
AN/TPQ-37	S	102	359	36,618	Hughes
Flap Lid	X	>100	10,000	>1 million	USSR
THAAD	X	2.5	25,344	63,360	Raytheon
COBRA	C	3	2,700	8,100	Lockheed

Commercial Satellite Communications

Customers for commercial satellite services include remote or mobile data-intensive professionals requiring fast downloading and uploading capabilities. Example users are banks, businesses using video-conferencing, oil drilling platforms, medical evacuation helicopters, airliners, cruise ships and the like. In developing countries, where a communications infrastructure is close to nonexistent, corporations are in need of ways and means to communicate. However, the greatest growth in demand may be fueled by consumer (residential) requirements such as: distance learning, electronic mail, home shopping, telecommuting, and entertainment services such as high definition television and video phones. Compared to geostationary (GEO) satellites, LEO satellites offer at least three major advantages. First, they orbit at an altitude generally below 1,000 km instead of about 35,000 km. Since signal loss is proportional to distance squared, an automatic power savings of about 30 dB occurs. This permits substantially smaller Earth terminals. Second, their proximity provides a nearly imperceptible propagation delay just like terrestrial systems, instead of the 0.25 second delay associated with GEO satellites. While this may be nothing more than a nuisance for voice services, it causes technical problems with higher data rates (for example, computer networking) and handshaking (for example, ATM switching). Third, there is potential for significantly reduced launch costs. For practical, aesthetic, or technical (agility and reliability) reasons, scanning phased arrays seems to be the lynchpin. System architectures tend to place considerable burden on the space segment, allowing the use of relatively small (for example, < 1 m) Earth terminals, to support data rates from perhaps 2.048 to 155.53 Mbps. These quixotic visions have yet to be realized, but could become tractable given a *low-cost* phased array solution.

There are also high data rate GEO platforms such as Spaceway (Hughes). Mobile platforms requesting service need some type of articulated antenna to track the satellite, both because of variable latitude and longitude, and to compensate for pitch, roll, and yaw. Again, the low-cost phased array seems an elusive solution.

Automated Highway Systems

At the turn of the millennium, there were about 140 million automobiles just in the United States. As populations grow, highway traffic expands, but construction costs and available real-estate prevent the highway system from keeping pace. The Intelligent Vehicle Highway System, especially in the context of intelligent cruise control, collision avoidance radar, and electronic tolling is a solution to optimize traffic flow and reduce flawed decision making. For a collision warning application, the phased array can be relatively small. Preliminary specifications suggest an operating frequency of 77 GHz with a 1.5° by 6° beamwidth, a 10 Hz scan rate, and 10 mW output power (ref. 3). Electronically-steered arrays enhance collision avoidance radar both because of the beam-pointing precision requirements, and the need to

essentially see around corners. The specified transmitter power corresponds to a timely warning for detecting a human, with a 1 m^2 radar cross-section, at a 300 m range (ref. 4).

Phase Shifter Characteristics

Evolving high data rate communications systems demand greater attention to subtle aspects of information theory and electromagnetic engineering. As the ratio of signaling bandwidth to carrier frequency decreases, less familiar phenomenon can influence system performance. And, new coding techniques are pushing channel capacity ever closer to the Shannon limit (ref. 5). Some interesting effects are expected to appear if the trend toward wide-band scanning phased array antennas and efficient high-speed modulators continues (ref. 6). For example, in a phased array antenna inter-element spacing, the physical size of the array, and the steering vector can conspire to introduce pulse distortion from group delay, inter-symbol interference, and beam squinting (refs. 7 and 8). And the operating point of the amplifiers can affect the bit error rate depending on the modulation type and the number of carriers. Naturally one wants the phased array to operate as efficiently as possible given power limitations and thermal management problems. This desire necessitates that the power amplifiers operate in a nonlinear region near saturation. Nonlinear effects cause amplitude-to-amplitude modulation (AM/AM) and amplitude-to-phase modulation (AM/PM) distortion. The net effect of AM/AM distortion is to alternately compress and expand the signal constellation. The net effect of AM/PM conversion is a rotation of the signal constellation (ref. 7). In a receive array, the third order intercept of the low noise amplifiers largely determines inter-modulation distortion and heat dissipation (ref. 9). But the phase shifter insertion loss envelope and phase accuracy are also key factors influencing array performance. Phase shifters typically follow low noise amplifiers in a receive array and precede power amplifiers in a transmit array. Since the phase shifter's insertion loss depends on its phase setting and since its switching action represents some finite time domain response, its potential contribution to bit error rate degradation cannot generally be ignored. There will always be some effects in any phase-shift keyed (PSK) modulation system, the degree to which depends on the steering vector update rate and data rate. A long switching time also increases minimum radar range. Besides these issues, the satellite communication market's desire to install tracking terminals on commercial mobile platforms, even at small office/home office and residential sites, has inspired the search for inexpensive phase shifters and affordable phased arrays. In practice, system constraints on chip size, power handling, drive power, insertion loss, bandwidth, phase error, transient response, and cost dictate particular device designs

Semiconductor

Semiconductor phase shifters, based primarily on GaAs, but also on SiGe and InP, have enjoyed steady progress for the past two decades. Their small size and relatively low power consumption compared to ferrite devices has created new insertion opportunities. Many possible circuit topologies, using diode or FET switches in various configurations, exist.

High-Pass/Low-Pass

In principle, any variable reactance in series or shunt across a transmission line can be used to introduce phase shift. A high-pass/low-pass phase shifter π network using discrete capacitors and inductors is shown in figure 1. In the high-pass configuration shown, a relative delay is realized. In the opposite configuration, with all SPDT switches toggled, the low-pass circuit represents a relative phase advance (ref. 10). It can be shown that if the circuit is matched, $X = 2B/(1 + B^2)$ and the insertion phase is $\tan^{-1}(2B/(B^2 - 1))$ (ref. 11). The switches can be implemented with PIN diodes or MESFETs, which will discussed later on in this section. It is possible to realize a phase shift of 180° with about 20 percent bandwidth.
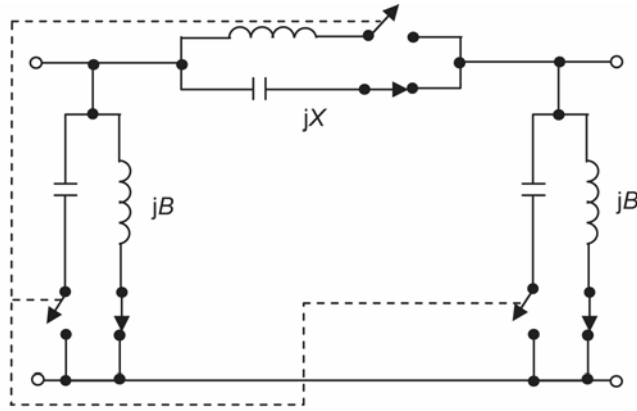
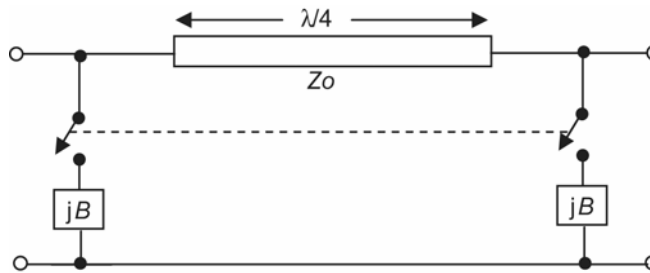Figure 1.—Topology for a high-pass/low-pass π network phase shifter. A dual "T" network realization is also possible.

Figure 2.—Loaded-line phase shifter.

Loaded Line

Another type of phase shifter generally used for achieving 22.5° to 45° of phase shift is the loaded-line (ref. 12). A schematic of this is shown in figure 2. Ideally, reactive loads spaced one-quarter wavelength apart are shunted across a transmission line to effect phase shift. The purpose of the second shunt susceptance (jB) is to cause a reflection, which will at least partially cancel the reflection from the first shunt susceptance (jB). By equating the ABCD matrix of figure 2 to an equivalent section of transmission line with electrical length θ_L radians and characteristic impedance Z Ohms as given in equation (1),

$$\begin{pmatrix} 1 & 0 \\ jB & 1 \end{pmatrix} \begin{pmatrix} 0 & jZo \\ j/Zo & 0 \end{pmatrix} \begin{pmatrix} 1 & 0 \\ jB & 1 \end{pmatrix} = \begin{pmatrix} \cos(\theta_L) & jZ\sin(\theta_L) \\ j\sin(\theta_L)/Z & \cos(\theta_L) \end{pmatrix} \tag{1}$$

we obtain

$$Z = Zo \Big/ \left[1 - (BZo)^2 \right]^{1/2} \tag{2}$$

and

$$\theta_L = \cos^{-1}(-BZo) \tag{3}$$

If the susceptance is capacitive, the phase velocity is decreased; if the susceptance is inductive, the phase velocity is increased. Loaded line phase shifters are inherently narrow-band and produce a constant phase shift versus frequency response. The phase versus frequency response is generally not as flat as the high-pass/low-pass type.
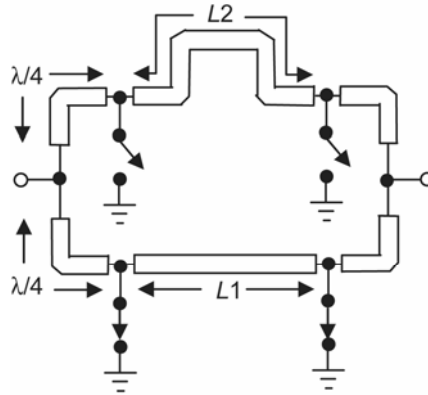
Figure 3.—Switched-line phase shifter. Signal path is through the delay transmission line with the switches set as shown.
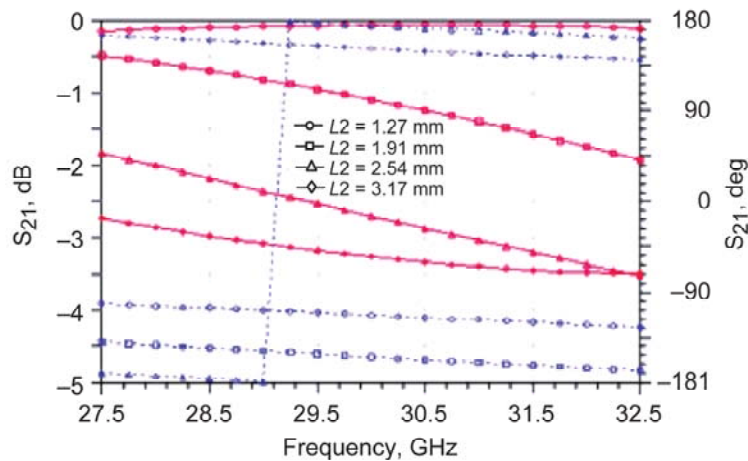

Figure 4.—Modeled insertion loss and phase with path $L2$ as as parameter. The red line is loss, and the blue line is phase.

Switched Line

The switched-line phase shifter is yet another popular type, and is intuitively easy to understand. SPDT switches are used to toggle between transmission lines with different path lengths. As opposed to the types discussed previously, this one is a true time-delay device. That is, it provides a phase response (φ) proportional to frequency (ω). Since time delay, $\tau = -d\varphi/d\omega$ and φ is proportional to ω, τ is a constant over the bandwidth. A schematic is shown in figure 3. The differential phase shift is

$$\Delta\varphi \approx \beta(L2 - L1) \tag{4}$$

where β is the propagation constant of the transmission line. As usual, β equals the radian frequency ω divided by v_p, where v_p is the phase velocity. A point of caution needs to be made with regard to this design, however. Utilizing series diode switches, it is possible that the off path length and switch capacitance can conspire to create a through path in parallel with the on path, resulting in high insertion loss and abrupt phase change in band. Utilizing MESFETs in place of the SPDT switches shown, the on path could also experience high loss under certain conditions. If the MESFET is treated as a very small resistance in series with a pinch-off capacitance of 0.1 pF, the insertion loss (and phase) of the "on" path, say $L2$, will vary as shown in figure 4 with $L2$ as a parameter.
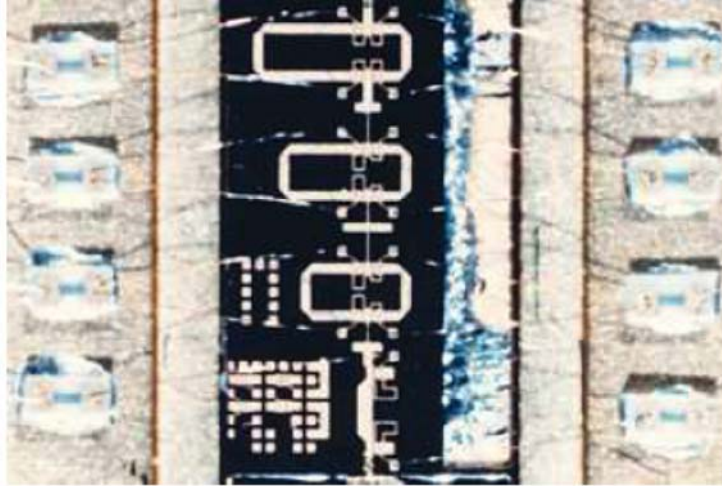
Figure 5.—30 GHz GaAs MMIC phase shifter using 1- by 400 mm switching FETs. The chip size is 5.5- by 2.5- by 0.15 mm^3 not including off-chip capacitors (after J. Geddes et al.[13] © IEEE, 1987 Ref. 13).

The higher loss with increasing $L2$ is predominantly due to interaction with the switches, not dissipative loss. So $L1$ and $L2$ must be chosen with deference to the switch characteristics.

A photograph of a 4-bit GaAs monolithic phase shifter is shown in figure 5 (ref. 13). The chip size is approximately 5.5- by 2.5- by 0.15-mm^3. The 180°, 90°, and 45° bits are implemented using the switched line approach, whereas the 22.5° bit is realized with a loaded line. The operating frequency was 30 GHz with about a 10 percent bandwidth. Average insertion loss was <10 dB with an insertion loss envelope of about 2 dB.

Beam Squint

A clear advantage of a constant time-delay is that beam steering is independent of frequency. For simplicity, consider a linear array of N elements separated by distance d (ref. 14). The incremental phase shift between adjacent elements to form the beam at an angle θ from boresight is

$$\Delta\varphi = \left(-2\pi d/c\right)f\sin(\theta) \qquad (5)$$

where f is frequency and c is the speed of light in vacuum. If the frequency changes by Δf, the beam squint angle $\Delta\theta$ and phase deviation $\delta\varphi$ are related by

$$\left(\Delta\varphi + \delta\varphi\right) = \left(-2\pi d/c\right)\left(f + \Delta f\right)\sin(\theta + \Delta\theta) \qquad (6)$$

If the phase shifter insertion phase is proportional to frequency, the beam squint $\Delta\theta$ is zero. If the phase is independent of frequency, however, $\delta\varphi$ is zero and equations (5) and (6) must be equal, yielding

$$f\sin(\theta) = \left(f + \Delta f\right)\sin(\theta + \Delta\theta) \qquad (7)$$

which causes a beam squint angle

$$\Delta\theta = -\theta + \sin^{-1}\left[\sin(\theta)/\left(1 + \Delta f/f\right)\right] \qquad (8)$$

Hence, wide scan angles and wide bandwidths correspond to significant scanning errors. In practice, phase shifters generally provide 0 to 2π phase shift. In electrically large arrays, the integer portion N of total delay required for true-time delay beam steering may be omitted, resulting in degraded performance.

In radar systems, where narrow pulses are required for high resolution, there is a correspondingly wide frequency spectrum. The effect of this modulo-2π problem is considered in detail later in this chapter.

Digital Control

The distribution of amplifier and phase shifter control signals in a large phased array is a complex problem. Thousands of MMIC modules must be interconnected into the beam forming manifold. Some type of digital interface circuitry must be used to address individual phase shifters and decode their control signals. The multiplexed data rate to accommodate fast scanning may approach a Gb/s (ref. 15). In one instance, a GaAs optoelectronic integrated circuit was used to detect and demultiplex an optical serial control signal into 16 parallel electrical signals (ref. 16). Operation of a Ka-band, 4-bit phase shifter at 30 MHz clock speeds was demonstrated. Average optical power was 250 μW. In another instance, optically controlled switching and X-band phase shifting was demonstrated such that the optically controlled GaAs FET interacted directly with the microwave signal (ref. 17). The FET was illuminated by the focused output of a 5 mW, 670 nm, InGaAlP laser diode.

Switching Q

Key requirements for microwave phase shifters include bidirectional (or reciprocal) functionality, low power dissipation, and low insertion loss. The insertion loss of the switched line phase shifter in the previous section depends on the SPDT switch loss and transmission line loss. As we have seen, an SPDT switch can be realized by several possible combinations of SPST switches. Basically, the switch is intended to minimize insertion loss in one state, and maximize isolation in the other. There are two fundamental configurations for SPST switches: as a series impedance or a shunt admittance. These are illustrated in figure 6.

Defining insertion loss as the ratio of available power delivered by the generator, to the load in the absence of the switch, to the actual power dissipated by the load in the presence of the switch, the insertion loss for the series (L_{se}) and shunt (L_{sh}) switch is

$$L_{se} = 20\log\left|1 + \frac{R_{sw} + jX_{sw}}{2Zo}\right| \text{ dB} \qquad (9a)$$

$$L_{sh} = 20\log\left|1 + \frac{(G_{sw} + jB_{sw})Zo}{2}\right| \text{ dB} \qquad (9b)$$

In general, Z_{sw} and Y_{sw}, and Zo for that matter, are frequency dependent. The swing in Z_{sw} and Y_{sw} determine insertion loss and isolation. Of course, the diodes and MESFETS used to realize the switches are inherently nonlinear. Diodes are forward- and reverse-biased, in order to produce the maximum possible change in impedance. In the forward bias state, the impedance is small, but the diodes conduct substantial dc current. In the reverse bias state, a depletion region is formed. It's worth noting that according to well-accepted theories for junction capacitance Cj, as forward bias is increased, Cj grows unbounded. Of course, capacitance is a measure of stored charge, and as the depletion region shrinks towards zero dimension, the stored charge diminishes towards zero (ref. 18).
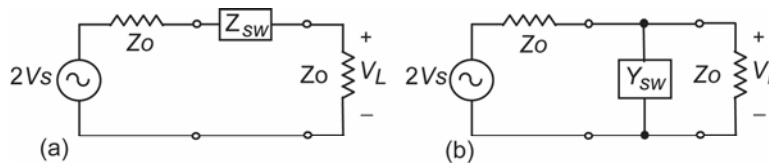

Figure 6.—Equivalent circuit for series (a) and shunt (b) single pole, single through switch. The switch impedance and admittance are $Z_{sw} = R_{sw} + jX_{sw}$ and $Y_{sw} = G_{sw} + jB_{sw}$, respectively.
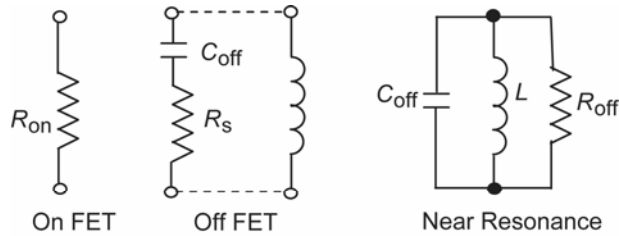
Figure 7.—Ideal equivalent circuits for on and off FETs. The inductor L is a short section of a transmission line used to parallel resonate the RC combination in order to enhance the high impedance state.

GaAs MESFET devices have replaced diodes in many switching applications. Monolithic integration advantages and lower power consumption are incentives. A FET is basically a gate voltage controlled resistor. Insertion loss is largely dictated by channel resistance, and gate-to-source capacitance determines isolation. To increase isolation (high impedance off state), a short (inductive) section of a transmission line is connected between the source and drain to resonate out the pinch-off capacitance C_{off} (refs. 19 and 20). Ideal equivalent circuit models for on and off FETs are shown in figure 7.

The resistor R_s is the total series resistance at pinch-off (undepleted channel resistance plus source and drain contact resistance). Sokolov (ref. 20) defined a figure of merit (Q) for switching FETs based on the work of Kurokawa and Schlosser (ref. 21) for a device switching between two impedance states Z_1 and Z_2, such that

$$Q^2 = \frac{|Z_1 - Z_2|^2}{r_1 r_2} = \frac{(R_{on} - R_s) + (\omega C)^{-2}}{R_{on} - R_s} \tag{10}$$

Here, r_1 and r_2 are the resistive components of the two impedance states. For the FET switch, $Z_1 = R_{on}$ and $Z_2 = R_s - j(\omega C_{off})^{-1}$. Assuming $(R_{on} - R_s) \ll (\omega C_{off})^{-1}$, a good approximation to equation (10) is

$$Q^2 = (R_{on} R_s)^{-1} (\omega C_{off})^{-2} R_{off} / R_{on} \tag{11}$$

Notice that Q degrades as the square of frequency. A high figure of merit requires small R_{on}, R_s, and C_{off}. Scaling the gate width allows a trade off between isolation and insertion loss. If the gate width is doubled, R_{on} and R_s are halved, C_{off} is doubled, and Q is invariant. Typical values of Q^2 at 10 and 30 GHz are about 1000 and 100, respectively. In normal operation, no bias is applied to the drain. A negative bias on the gate (relative to the source) pinches off the channel. Zero or positive gate bias turns the channel on. Additional information on switching Q and its relationship to loss is provided in the reference section (refs. 22 and 23).

Thin Film Ferroelectric

Serious research on bulk (waveguide) ferroelectric phase shifters began in the 1960s but poorer performance in comparison to ferrite devices, coupled with very high tuning voltages, forestalled industrial acceptance. New thin film deposition techniques and novel circuit designs in the 1990s heralded a new generation of devices rivaling their semiconductor counterparts in essentially every figure-of-merit.

Materials and Basic Properties

In a ferroelectric material, such as $Ba_xSr_{1-x}TiO_3$, applying a dc electric field shifts the position of the central Ti atom in the crystal, resulting in a net dipole moment on a macroscopic scale (ionic polarization). Analogous to ferromagnetic materials, domains form in the material where the dipoles are

locally aligned (orientational polarization). The Ti ion can remain shifted even after the applied field is removed, and the domains can move in response to applied ac and dc fields. Microwave phase shifters are generally operated above the Curie temperature, in the paraelectric state. Ideally, this means operating without residual polarization and domain formation, thereby reducing hysteresis and dielectric loss. The Curie temperature, which represents a phase change to a nominally cubic crystal lattice, can be tailored for a specific operating temperature by adjusting the composition of $Ba_xSr_{1-x}TiO_3$ (BST), where $0<x<1$, and for room temperature $x \approx 0.60$. Interest in ferroelectric-based agile microwave circuits is mounting because of their high power handling capability, negligible dc power consumption, and potential for low loss and cost. The ferroelectrics discussed here belong to the perovskite crystal family. The dielectric constant (ε_r) of single crystal $SrTiO_3$, an incipient ferroelectric, can be depressed from about 20,000 to 2,000 with a dc field of 10^4 V/cm at 4.4 K (breakdown voltage for the materials of interest here is $>10^5$ V/cm) and the loss tangent maintained below 0.1 percent. Thin films of $SrTiO_3$ exhibit $\tan\delta$ as poor as 0.01 with a peak relative dielectric constant of $\approx$5,000. The dielectric constant also tends to exhibit a broad maximum with temperature as opposed to bulk material. The differences in behavior have been attributed to residual domain wall motion, compositional inhomogeneities, interface layers between the film and electrodes, and lattice mismatch induced stress. Fundamental loss mechanisms have been considered in some situations (ref. 24). Attempts to reduce $\tan\delta$ have included annealing, which tends to increase grain size, and the use of dopants, which may reduce free charge or otherwise affect loss mechanisms (refs. 25 to 27).

Several ferroelectric phase shifters have been developed with varying success. A stripline circuit with a BST capacitor provided a differential phase shift of 11° at X-band with a biasing field of 70 kV/cm (ref. 28). In that same work, a center-wire bias waveguide phase shifter produced more than 360° of phase shift at Ku-band by changing the bias between the wire and waveguide walls from 0 to 2,500 V. A planar microstrip phase shifter was reported that provided 20°/kV at 2.65 GHz (ref. 29). A phase shift of 165° at 2.4 GHz with only 3 dB loss and a bias of 250 V was obtained from a microstrip on a thin BST slab synthesized using a sol-gel technique (ref. 30). There was also a 40 GHz phased array antenna that used radiating slots in waveguide and a BST film sintered onto a MgO substrate (ref. 31). Voltage applied across a periodic set of electrodes changed the dielectric constant of the BST from 700 to 1,500 and a $\tan\delta$ of 0.05 was reported. A ferroelectric lens that uses BST slabs sandwiched between conducting plates was also proposed (ref. 32). The approaches advanced thus far have not been able to simultaneously address low cost, low loss, and small size. And in some cases, the impedance variation, due to widely changing permittivity, posed additional difficulties. Two promising implementations include coupled line and synthetic line-based devices, to be discussed next.

Coupled Microstripline

Another style of phase shifter uses coupled microstriplines as dc electrodes to polarize a thin ($\approx$0.4 μm) ferroelectric film. With $YBa_2Cu_3O_{7-\delta}$ electrodes and 2.0 μm thick $SrTiO_3$ films, this phase shifter produces a figure of merit approaching 120°/dB at 40 K (ref. 33). At room temperature, using Au electrodes and 400 nm thick $Ba_{1-x}Sr_xTiO_3$ films devices have demonstrated $\approx$70°/dB (ref. 34). These planar phase shifters are fairly compact, low loss, easy to fabricate, and can provide 360° of phase shift with bias voltages under 350 V. Such devices can enhance conventional (direct radiating) phased array performance or enable a new type of reflectarray antenna (ref. 35 and 36). Only one control line is required per phase shifter, thereby simplifying array assembly. A variation is a hybrid X-band phase shifter consisting of four cascaded coupled microstrip lines, patterned over 400 nm thick laser-ablated $Ba_{0.50}Sr_{0.50}TiO_3$ films, followed by a switch (ref. 37). The ferroelectric section provides (nominally) 180° of analog phase shift. Basically, as a bias from 0 to 350 V is applied across the coupled line electrodes, the relative dielectric constant of the film tunes from about 2000 to 800, thereby modifying the propagation constant. The ferroelectric films are, of course, excellent dielectrics and the current draw is negligible so there is virtually no power consumption. Switching speed for these devices is limited by the external power supply. This is analogous to MESFET switches, wherein there is no drain bias. The
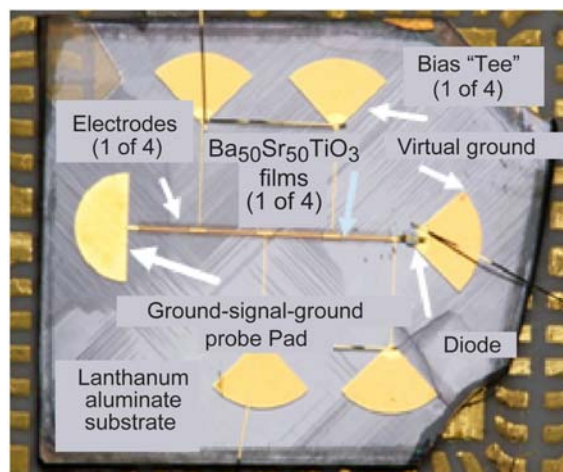
Figure 8.—Hybrid X-band ferroelectric/semiconductor
phase shifter on 0.5 mm thick lanthanum aluminate.
The device measures ≈ 1- by 1-cm.

variable resistance of a FET switch is a function of the population of majority carriers, as opposed to minority carriers in PIN diodes. (For example, in FET switches, speed is not limited by minority carrier lifetime, but rather the gate control circuitry). The beam lead GaAs diode switch is appended to the last coupled microstrip section and toggles between an open and virtual short circuit, realized with a quarter-wave radial stub. This results in a "digital" transition between a reflection coefficient with magnitude near unity and phase of ≈0° and ≈180°, respectively. Thus, a full 2π phase shift is possible. The average loss at X-band was 3.2 dB with a 10 percent bandwidth. The device is pictured in figure 8. Note that the unmatched beam-lead diode contributed 0.5 to 0.75 dB to the overall insertion loss. In principle, this can be improved by "resonating-out" the diode capacitance.

Theory of Coupled-Line Type

A sketch of the cross-section of a coupled-line (multi-dielectric-layer) ferroelectric phase shifter is shown in figure 9. Y_1 and Y_2 represent the admittance looking in the positive and negative y direction, respectively, from the charge plane. The thickness of the ferroelectric layer is h_1 while the host substrate has thickness h_2.

By concentrating the fields in the odd mode, the phase shift per unit length is maximized and by using the material in thin film form the effects of high loss tangent are reduced.

The amount of phase shift can be increased by cascading coupled line sections. Though methods for calculating the propagation parameters of coupled transmission lines are well known, coupled lines on stratified substrates are difficult to analyze. And the high permittivity of the ferroelectric layer causes long computation time by full-wave electromagnetic simulators because the geometry must be fractured into many thousands of cells. The multilayer structure has been analyzed using a computationally efficient variational method for calculating the complex propagation constant and characteristic impedance (ref. 38). Space limitation prevents a full description of that work here. However, the method is quite general and can be used for multiple layers of various dielectrics or other types of transmission lines. For example, a multi-layer microstrip can be analyzed by allowing the strip spacing (s) to become much greater than the effective substrate thickness (h) or strip width (w). Minimum loss occurs when current flows through one line and returns through the other (odd-mode), obviating the need for the ground plane. Maximum loss occurs when equal currents flow through the two lines and return through the ground plane (even-mode). Three basic modes are illustrated in figure 10.
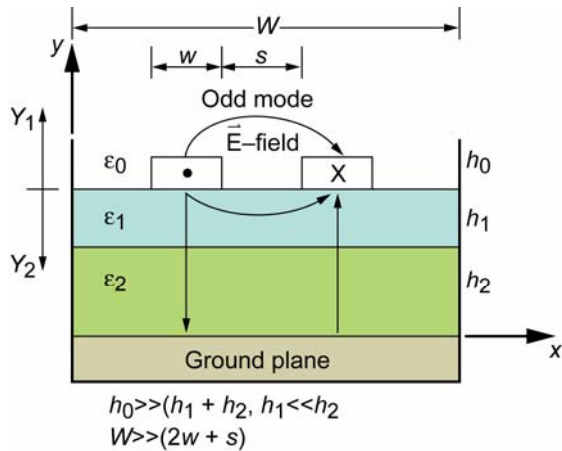
Figure 9.—Cross-section of the coupled micro-stripline phase shifter, showing the odd-mode electric field configuration.
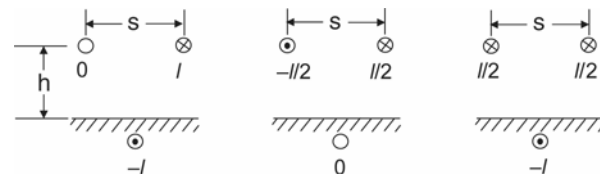

Figure 10.—Coupled line modes: microstrip mode (left), $s \gg h, w$; odd-mode (middle); even-mode (right).

Note that the ferroelectric layer thickness is crucial to performance. In principle, the phase shift for a 2 µm thick film is 2.2 times greater than that of a 0.5 µm film. However maintaining the crystalline quality of the pulse laser ablated $Ba_xSr_{1-x}TiO_3$ films past a thickness of 0.5 µm or so has proven to be difficult. Experiments have shown that the insertion phase shift is roughly proportional to $h_1^{0.67}$. In the case of cascaded coupled lines, increasing phase shift occurs at the expense of bandwidth since the structure resembles a multi-pole filter. Changing the dielectric constant of the ferroelectric film to change its insertion phase also modifies the pass band characteristic. Operation near band edges is to be avoided since that represents distorted transmission which degrades bit-error-rate performance. The device discussed in the previous section "Coupled Microstripline" helps alleviate this problem. The impedance matrix of the cascade network can be derived by traditional coupled line theory, using the superposition of even and odd mode excitation. Then an equivalent S-parameter model can be extracted and used to predict the pass-band characteristics of the phase shifter. A key advantage of this technology is the relatively large feature size. Active devices at the frequencies of interest here would necessitate submicron gate length GaAs FETs. The finest feature size associated with the coupled-line phase shifters is the electrode separation, typically ≈10 µm. Whereas the GaAs FET performance is largely dictated by transconductance, and hence, carrier transit time across the gate region, the coupled-line phase shifters are static devices. The electrode gap separation determines the degree of electromagnetic coupling and the dc potential required to tune the film.

Micro-Electro-Mechanical Systems (MEMS)

MEMS can essentially be used to replace PIN diode or FET switches in conventional phase shifters. A typical switch consists of a metal membrane bridge suspended several microns above a lower metal contact. Electrostatic attraction between the flexible membrane and lower contact is used to toggle the switch. A very thin dielectric coating (for example, Si_3N_4) may be used on the lower contact to eliminate a dc path and reduce "stiction," or a tendency to latch (also known as Van der Waals forces). Larger bridge heights (gaps) reduce parasitic capacitance, but increase pull-down voltage and may contribute to more fatigue. Typical actuation voltages are between 20 and 100 V. An interesting advantage of MEMS switches is that they do not depend on the characteristics of the substrate. Hence, they may be fabricated on any material that is compatible with standard IC processing. A photograph of one type of MEMS switch is shown in figure 11. Optimizing the switching Q amounts to minimizing the parasitic capacitance of the bridge in the off state (bridge up), and maximizing capacitance in the on state (bridge down). When
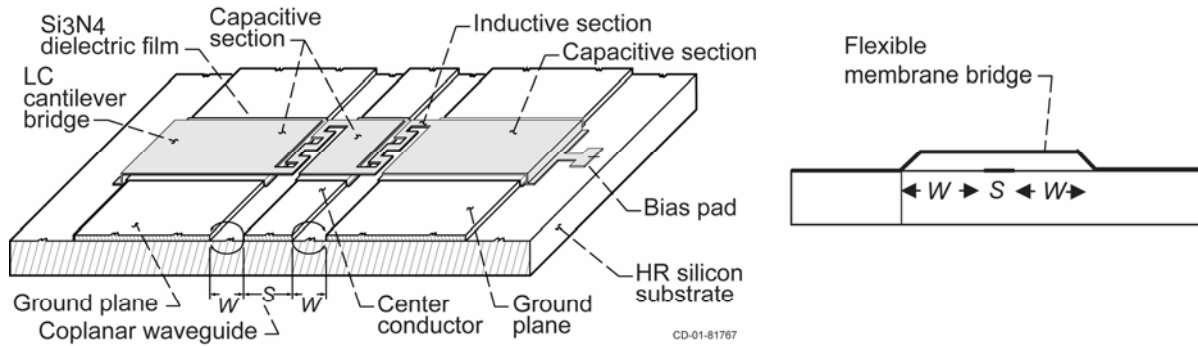
Figure 11.—RF MEMS capacitive switch. MEMS devices incorporating capacitive\inductive sections allow the switch to be designed for minimum loss and maximum isolation over a wide frequency range (after M. Scardelletti[43] © IEEE 2002).

the cantilever is down, the parallel plate capacitance between the metal membrane and the bottom electrode, C_{on}, is large and the switch behaves as a short circuit. Typical ratios of C_{on}/C_{off} are ≈ 100.

A number of distributed MEMS transmission line phase shifters have been developed (ref. 39). An insertion loss of 4 dB at 60 GHz (for a full 360° phase shift) and 257°/dB at 50 GHz has been reported (refs. 40 and 41). These excellent results have been obtained from MEMS bridge capacitors placed periodically along a coplanar waveguide (CPW) transmission line. The theory of such "slow-wave" circuits is discussed in the next section. Activating the MEMS increases the capacitive loading, thereby controlling the insertion phase. A mechanical analysis of operation was provided (ref. 42) and the bridge spring constant was given as

$$k \approx 32Et^3\, w/(S + 2W)^3 + 8\sigma(1 - \upsilon)tw/(S + 2W)\ \ N/m \tag{12}$$

where E is Young's modulus of the bridge material, t is the bridge thickness, w is the bridge width, S is the CPW center conductor width, W is the CPW center conductor-to-coplanar ground spacing, σ is the internal residual stress of the bridge, and υ is Poisson's ratio. The pull-down voltage V_p is given as

$$V_p = \left[8kg_o{}^3/(27\varepsilon_o Sw)\right]^{1/2}\ \ V \tag{13}$$

where ε_o is the free-space permittivity and g_o is the zero-bias bridge height.

One issue with MEMS phase shifters is that packaging is perhaps more critical than with alternative technologies. Hydrocarbon contamination may compromise MEMS reliability so hermetic seals and careful processing are required. A summary of performance and implications for phased arrays are presented in the reference section (refs. 44 and 45).

Slow-Wave

Periodically loaded transmission lines are used to realize band-pass, slow-wave circuits such that $v_p \ll c$. By using tunable loads or varactors, broad-band phase shifters can be designed.

One-Dimensional Periodic Structures

Consider a cascade of short sections of lossless transmission line shunted by a voltage variable capacitance C', so as to form the infinite periodic structure illustrated in figure 12. Each distributed transmission line section is modeled by an LC circuit and each unit cell consists of L, C, and C'. Let the separation of each unit cell be designated as s. Such periodic structures exhibit slow-wave behavior ($v_p \ll c$) and band-pass characteristics, like filters. The phenomenon is analogous to acoustic wave propagation in crystal structures. These types of circuits are often referred to as synthetic line, slow-wave, or distributed transmission line phase shifters.
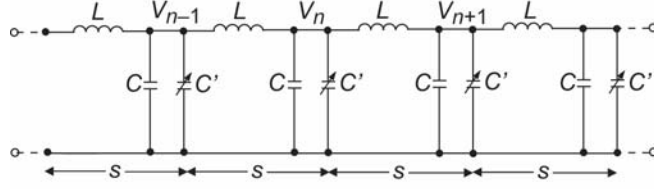
Figure 12.—A chain of *LCC'* circuits representing an infinite, periodically loaded transmission line resulting in slow-wave propagation.
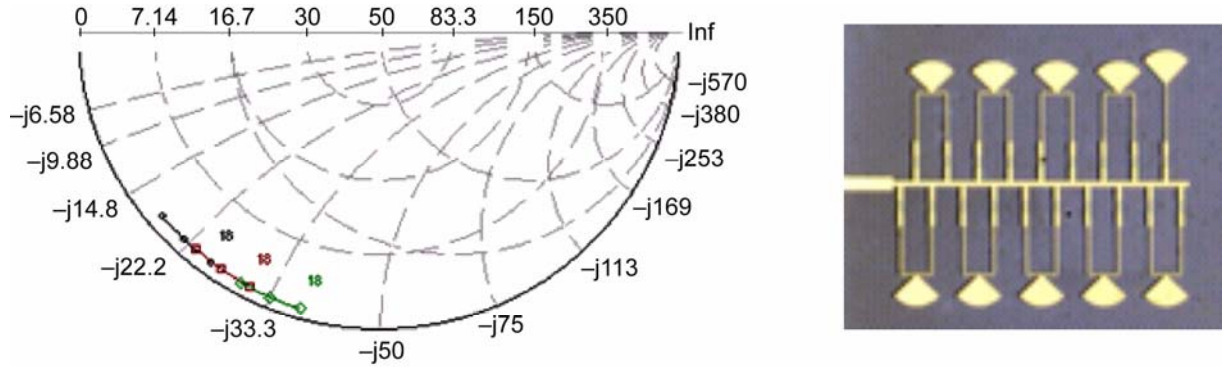

Figure 13.—Modeled impedance variation of a 19 cell slow wave circuit from 18 to 20 GHz as the ferroelectric film dielectric constant varies from 2000 to 800 (left). The actual circuit (right) had a 0.6 mm cell size with 200 mm long coupled-line varactors.

A wave traveling through this periodic structure will only experience a phase shift from unit cell to unit cell, such that V_n is delayed relative to V_{n-1} as

$$V_n = V_{n-1}\ e^{-j\theta s} \tag{14}$$

In general, θ_s could be complex to account for attenuation as well as phase shift. Summing currents leaving node n

$$0 = V_n\left(j\omega C + j\omega C'\right) + \left(V_n - V_{n-1}\left(-j/\omega L\right)\right) + \left(V_n - V_{n+1}\left(-j/\omega L\right)\right) \tag{15}$$

Substituting equation (12) into equation (13) we arrive at

$$\cos(\theta_s) = \tfrac{1}{2}\left(2 - \omega^2 L\left(C + C'\right)\right) \tag{16}$$

Requiring θ_s to be real to represent a propagating mode, letting $\cos(\theta_s) = \pm 1$, we find the structure of figure 12 has a zero lower frequency cutoff ω_L (obvious by inspection) and an upper cutoff frequency ω_H corresponding to

$$\omega_H = 2/\left(L\left(C + C'\right)\right)^{1/2} \tag{17}$$

Since $\theta_s = \beta s$, the insertion phase shift can be approximated knowing the extremes of the tuning range of C' and the number of cascaded sections. Slow wave phase shifters are, in principle, time delay devices (in other words, phase shift is proportional to frequency).

Ferroelectric Varactor

One type of slow wave phase shifter, based on ferroelectric "varactors" is shown in figure 13. Coupled lines, as described in the previous section called "Theory of Coupled-Line Type," are attached

transversely to the propagation direction in a microstrip configuration (ref. 46). A unit cell consists of two microstrip sections, with an intervening orthogonal coupled microstrip line terminated in a virtual open circuit. The open circuit is realized by cascading a nominally quarter-wave high-impedance microstrip line, having impedance Zp, with a radial stub. The stub provides a very good approximation to a short circuit at its vertex, over almost an octave bandwidth, and the input impedance (Zin) to the combination is approximately 35 Zp/α, where α (dB/λ) is the attenuation of the Zp line. Note that there is an optimal choice for Zp since as Zp increases to maximize Zin, α also increases due to conductor loss.

For the reactances chosen and shown, the modeled dissipative loss was about 0.125 dB/unit cell. There is a trade-off between loss and phase shift. For a median varactor reactance of –j500, the calculated loss per unit cell is 0.003 dB, but the phase shift is also $\ll$1°/cell and appears impractical. For a reactance of –j5 the insertion loss is about 8.6 dB/cell and is also impractical. For the K-band circuit shown, the varactors theoretically tuned from 0.45 pF (zero bias) to 0.25 pF (maximum bias), and 16 unit cells should have provided 360° of phase shift at 20 GHz. These results could be obtained using the techniques described in the subsection entitled "Coupled Microstripline." The measured phase shift of the actual 19 cell structure was about 250° with an average loss of about 7.5 dB.

Excellent results have been obtained from slow wave circuits using parallel-plate ferroelectric varactors (refs. 47 to 49). The circuits operating principles are basically as described in the Slow-Wave section. The device consists of a high impedance transmission line on sapphire, periodically loaded with $Ba_xSr_{1-x}TiO_3$ capacitors spaced by distance s. Recently, $\approx$ 360° phase shifters at K- and Ka-band exhibited an average loss of about 5 and 6 dB, respectively (ref. 50). One advantage of the parallel plate approach is that conventional tuning voltages can be used (for example, $\approx$10 V as opposed to > 100 V for coplanar structures). Another advantage is that circuits can be fabricated on convenient substrates like Si instead of exotic, high epsilon substrates like $LaAlO_3$. Propagation in semiconductor substrates has also been discussed (ref. 51). The circuits are also extremely compact. A Ku-band version measuring 1- by 0.8-mm was reported (ref. 50).

Ferroelectric deposition methods (for example pulse laser, sputtering, and so on) require an oxidizing atmosphere around 700 °C to achieve high quality crystalline films. Hence, electrodes for parallel plate varactors, as opposed to the coplanar or interdigital structures described previously, must be impervious to high temperature oxidizing atmospheres. Low dielectric constant oxides at the electrode interface can drop most of the electric field and substantially reduce tuning. Pt is a popular electrode material choice.

Ferrite

The fundamental source of a material's magnetic properties is the magnetic dipole moment associated with what is visualized as an electron spinning about its axis. In non-magnetic materials, the number of electrons with up spins and down spins is equal, so the net magnetic moment is negligible. In a magnetic material, one variety dominates and can be aligned by an external DC magnetic bias field H to generate a large magnetic moment, as long as thermal fluctuations aren't too strong. The spin magnetic moment vector precesses about the H-field vector at an angular frequency $\omega_m = 2\pi f_m$. Precession sense (i.e., polarization) depends on the direction of H. The precession frequency is proportional to H such that $f_m = \gamma H$, where $\gamma = 2.8$ MHz/Oe is the gyromagnetic constant. The propagation constant (β) in a ferromagnetic medium is

$$\beta \approx \left(2\pi\sqrt{\varepsilon\mu'}\right)/\lambda \tag{18}$$

where μ' is the real part of the permeability and ε is the dielectric constant of the ferrite. When the frequency f of a microwave magnetic field equals f_m, ferrimagnetic resonance occurs. This is the underlying cause for opposite circularly polarized waves experiencing different permeabilities, μ'_+ and μ'_-. In the absence of any loss mechanism, the material's susceptibility would become infinite at the gyromagnetic resonance frequency. The permeability can be tuned by changing M, which is the

magnetization or magnetic moment. As the strength of the magnetic bias field increases, M will reach an upper limit called the saturation magnetization, denoted as M_s. Ferrite materials tend to have high loss below saturation at microwave frequencies. The choice of ferrite for a particular application is determined by selecting $\gamma 4\pi M_s$ sufficiently below the operating frequency f. When f_m is small compared to f, there is a significant difference between μ'_+ and μ'_- for the two polarization senses. (Recall that a linearly polarized wave can be disassociated into two counter-rotating circularly polarized components.) With this condition, it can be shown that (ref. 52)

$$\mu'_\pm = 1 \mp \gamma 4\pi M / f \tag{19}$$

and the corresponding phase shift is

$$\Delta\varphi = 2\pi\sqrt{\varepsilon}\left[(\mu'_+)^{1/2} - (\mu'_-)^{1/2}\right] L / \lambda \tag{20}$$

where L is the length of the ferrite section. In practice, the phase shift is implemented by reversing the direction of the magnetization vector.

As was alluded to in the introduction, ferrite phase shifters have tended to dominate the phased array landscape. The basic, nonreciprocal, latching phase shifter consists of a toroidal ferrite core in a section of waveguide. A drive wire passes through its center, which is used to magnetize the material. At this point it becomes latched at one of two remanent states, depending on the polarity of the bias. The amount of differential phase shift between the two states is determined by the toroid length. Another common device is the reciprocal, non-latching Reggia-Spencer phase shifter. A ferromagnetic bar is located axially in a section of waveguide, which is wound by a solenoid. The solenoid produces a longitudinal magnetic field that changes the permeability of the bar material. The reader is referred to the previous edition of this book and the references therein for complete descriptions. The performance of twin-toroid, dual-mode, and rotary-field ferrite phase shifters has been discussed elsewhere (ref. 53).

Microstrip Type

Our interest here will be a brief introduction to microstrip-type ferrite phase shifters. Planar microstrip geometries promise an economical and small-sized replacement for waveguide phase shifters. For example, a small analog X-band stripline on a ferrite slab yielded a figure-of-merit of 300°/dB with a 30 mW average drive power (ref. 54). A renewed interest in this type of device was spurred on by the advancement of high-temperature superconductors, which are briefly discussed in the next section. The key advantage of superconducting transmission lines is the very low surface resistance compared to metallic conductors.

Low-loss microstrip ferrite phase shifters were demonstrated by combining the superconductor $YBa_2Cu_3O_{7-x}$ with polycrystalline yttrium iron garnet $Y_3Fe_5O_{12}$. The design confined the magnetic flux within the ferrite to avoid undesirable flux penetration into the superconductor, yet allowed gyromagnetic interaction with the microwave signal (refs. 55 and 56). A prototype phase shifter using a $YBa_2Cu_3O_{7-x}$ microstrip meander line deposited on a $LaAlO_3$ substrate is shown in figure 14.

A differential phase shift in excess of 200° with an insertion loss generally below 2 dB from 6 to 12 GHz was reported (ref. 52). Besides the insertion loss advantage of the superconducting line, the $4\pi M_s$ values can increase by more than a factor of two when the material is cooled from 300 to 77 K.
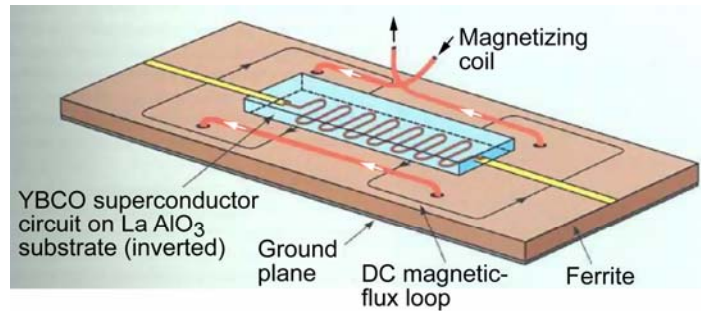
Figure 14.—Geometry for a superconducting microstrip meander line phase shifter inverted and in close proximity to a tunable ferrite substrate. The device is about 1.3 cm long (after G. F. Dionne et. al.[52] © Lincoln Laboratory, MIT 1996).

Superconducting Applications

While conventional or low temperature superconductor based phase shifters have been developed to some extent (refs. 57 to 58), the discovery of so-called "high-temperature" ceramic superconductors in 1986 (ref. 59) ushered in a new class of microwave components. High temperature superconducting (HTS) phase shifters are a subset of that class. The main attraction was dramatically reduced surface resistance compared to metallic conductors. The three primary HTS materials are $YBa_2Cu_3O_{7-x}$, $BiCaSrCuO_x$, and $Tl_2Ba_2Ca_2O_x$ with respective transition temperatures (T_c) of 95, 110, and 122 K. Surface resistance (R_s) of these superconducting films at 77 K is on the order of 100 µΩ at 10 GHz, compared to about 10 mΩ for copper.

The surface impedance of a superconductor is derived using a two-fluid model, which maintains that the current is composed of both superconducting (paired) and normal electrons. The proportion varies such that at $T = 0$, all carriers are superconducting and at $T = T_c$ all carriers are normal. The two-fluid model predicts that the surface resistance of a superconductor is proportional to f^2, as opposed to $f^{1/2}$ for a metallic conductor (ref. 60). The strong dependence of R_s on frequency is a consequence of reactive voltage, associated with the oscillating supercurrent interacting with unpaired (normal) electrons to induce loss. The corresponding (inductive) surface reactance is $\omega\mu\lambda_L$, where λ_L is the London penetration depth. λ_L has a minimum value at $T = 0$ and diverges as T approaches T_c. The abrupt change in resistance and kinetic inductance ($\mu\lambda_L$) near T_c presents opportunities for novel detectors (for example, transition edge bolometers) and switching mechanisms.

Reflective switches can be based on driving a narrow superconducting bridge into the normal state by locally exceeding the superconductor's critical temperature (ref. 61). Alternatively, a magnetic field on the order of 100 G was used to cause a small bar of $YBa_2Cu_3O_{7-x}$ to transition from the superconducting to normal state (ref. 62). The effects of optical illumination have also been investigated (ref. 62 and 63).

A novel phase shifter based on a HTS distributed Josephson inductance transmission line was reported (ref. 64). Superconducting quantum interference devices (SQUIDs), consisting of a superconducting inductor shorted by a Josephson junction, were distributed along a length of superconducting transmission line. Each SQUID can be modeled as a variable inductor, which is tuned by applying a magnetic field. The circuit constitutes a dual of the structure discussed in the Slow-Wave section. Slow-wave propagation in superconducting transmission lines has also been studied. For example, the dramatic increase in λ_L near T_c causes a large reduction in v_p if the film is very thin (ref. 65).

We conclude this section noting that the field of cryogenic electronics is growing and may be further stimulated by recent advances in compact, reliable, mechanical refrigerators. While a few esoteric systems have been created for space-based astrophysics, ultra-sensitive receivers, and medical diagnostics, there may also be niche applications in communications markets. Cryogenically cooled receivers for cellular phone towers are a good example. The enhanced sensitivity allows for increased

cell-size. It is easy to speculate that applications for cryogenically cooled agile antennas, and hence phase shifters, may also eventually exist. Digital beam-forming systems based on Josephson technology are also being contemplated.

Effect of Phase Shifter Behavior on Phased Array Bit Error Rate

Phase shifters' phase errors can cause some signal distortion, and phase transients can cause beam pattern degradation during direction switching. Signal models have been established for both static and transient cases. Moreover, modulo 2π effects cause intersymbol interference (ISI). This section is based on the work reported in this area (ref. 66).

Modulo 2π Effects

The composite far-field signal formed by a phased array is the summation of individual contributions from each elemental radiator. Radiation path lengths to the far-field observation point are different for each elemental radiator on the array surface. To form a cophasal beam, modulo-2π compensation is provided by the phase shifters. Integer-multiples of 2π are generally not provided, and for an electrically large array, this leads to inter-symbol interference (ISI) in phase-shift keyed modulation formats. The ISI is formed because different delays from each signal component destructively interfere, as illustrated in figure 15, for Binary Phase Shift Keyed waveforms. ISI results in composite (total) signal amplitude loss at the symbol boundary.

As an example, for the reflectarray (refs. 35 and 36) operating at $f = 26.5$ GHz with a bit rate of 1.325 Gbps, the BER degradation due to ISI is proportional to the symbol rate and the loss ranges are from about 1 dB to around 2 dB in E_b/N_o, depending on original E_b/N_o, for BPSK, QPSK, 8PSK, and 16QAM.
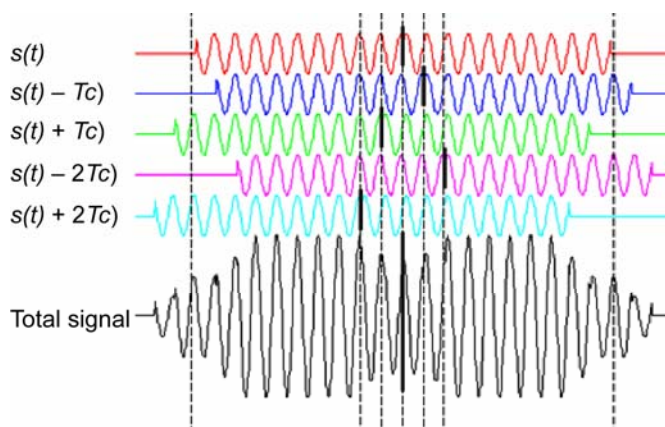

Figure 15.—Formation of ISI due to different delays in signal components. The carrier period is designated T_c. Heavy vertical lines are symbol boundaries (after F. Xiong and R. Romanofsky[67] © IEEE 2005).

Phase Errors

Each phase shifter assigned to each element is designed to shift the signal phase by an amount determined by the steering angles of the antenna. In practice, however, there are errors in the phase shifters. Assume that the phase errors are uniformly distributed in $\left[-\Delta\varphi_{max}, \Delta\varphi_{max}\right]$. It was shown in that the averaged effect of phase error is to introduce an amplitude loss of

$$L_{\Delta\varphi} = \frac{\sin\Delta\varphi_{max}}{\Delta\varphi_{max}} \quad \text{or} \quad L_{\Delta\varphi}(dB) = \left|20\log\left|\frac{\sin\Delta\varphi_{max}}{\Delta\varphi_{max}}\right|\right| \tag{21}$$

and there is no net phase shift of the composite signal due to the phase errors. For a maximum phase error of $\pi/8$, the loss is only 0.224 dB. It can be seen that the phase error loss is a sin$c$ function of $\Delta\varphi_{max}$ and it can be shown that the maximum phase error must be less than 47° to limit the loss within 1 dB.

The real composite signal will have not only amplitude loss, but possibly also a small net phase error. The small net phase error could have a degrading impact on the BER performance of the high-order PSK schemes and QAM schemes, since the phase differences between constellation points are very small.

Effect of Finite Response Time on Beam Evolution

Different types of phase shifters will have different transient response times. Table 2 provides a qualitative assessment. When the array beam is switched from one direction to another, the finite response time of the phase shifters causes the beam pattern to evolve. This effect is in addition to the ISI and phase error described earlier. The problem was analyzed by incorporating the phase transient in the array factor. For the 925 element array investigated there, which assumed a quite long 0.3 ms average phase shifter response time, the directivity degraded by a much as 1.9 dB during position updates.

Experimental results were reported (refs. 67 and 68) that would of course include all the effects described herein. Clearly, electrically large phased arrays communicating wide-band signals with high order modulation formats must be designed to compensate for these effects. A set of BPSK BER curves for various conditions is shown in figure 16 (transient effect excluded). The term "without antenna" means that the antenna is ideal—no phase errors and no ISI.
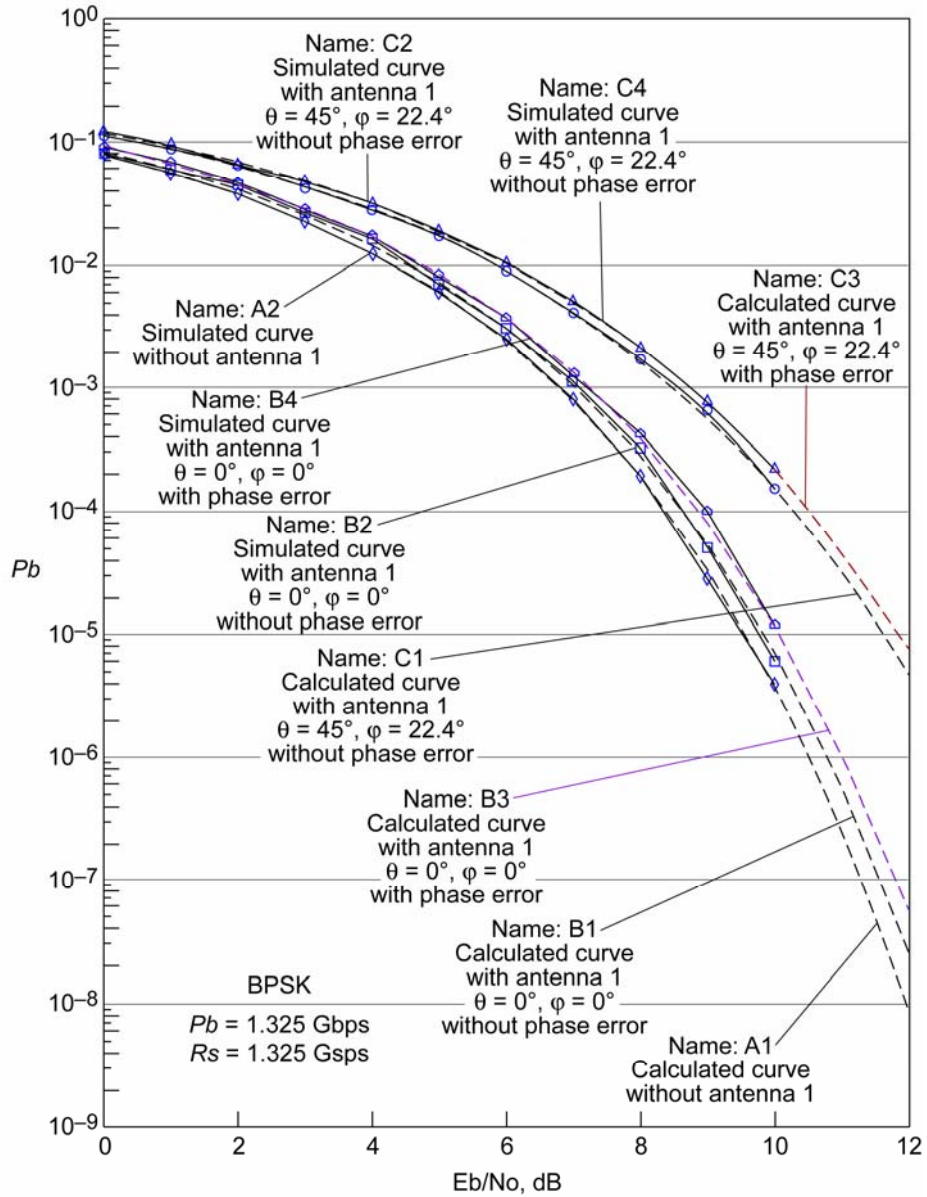
Figure 16.—BER curves for BPSK (after F. Xion and R. Romanofsky[67] © IEEE 2005).

TABLE 2.—COMPARISON OF PHASE SHIFTER TECHNOLOGIES

Type \ Feature	Ferroelectric	Semiconductor/ MMIC	Ferrite	MEMS
Cost	Low	Expensive	Very expensive	Low
Reliability	Good after 10^6 0 to 40 V/μm bias cycles (more tests required)	Very good (if properly packaged)	Excellent	Good after several billion cycles (more tests required)
Power handling	Good, >1 W	Very good, tens of watts	Very high (kW)	Low Power, <50 mW for high reliability
Switching speed	Intrinsically fast (≈ns), controller limited if high voltage	Fast at low power ($<10^{-9}$s)	Slow (inductance) 10 to 100 μs	Slow (mechanical) 10 to 100 μs
Radiation tolerance	Excellent	Poor (good if radiation hardened)	Excellent	Excellent (mechanical; no solid state junctions involved)
DC power consumption	Low ($\ll$1 μA current) μW	Low (<10 mW for diodes; negligible for FETs)	High (large current) ≈10 W (≈1 W if latching)	negligible
RF loss	~5dB/36° @ K-band	~2 dB/bit @ Ka-band = 8 dB	<1 dB /360° @ X-band	~2.3 dB/337.5° @ Ka-band
Size	Very small if parallel plate varactor (mm^2)	Small (≈10 mm^2 at Ka-band)	Large (wave-guide, bias coil)	Small (comparable to MMIC)
Linearity	IMD intersect +60 dBm	IMD intersect +35 to +40 dBm		IMD intersect +80 dBm

Summary

This chapter reviewed basic phase shifter theory and described some modern phase shifter devices. Key developments of the past decade or so include devices based on GaAs MMIC, MEMS, and thin ferroelectric films. Applications of superconductivity were also briefly described. Some interesting effects are expected to manifest themselves as the ratio of signaling bandwidth to carrier frequency decreases, especially with regard to electrically large phased arrays. An important aspect of phase shifter performance is power handling capability. The reader is referred to the reference section (refs. 69 to 72) for information on this topic. A summary of phase shifter characteristics is presented in Table 2.

References

1. E. Brookner, "Major Advances in Phased Arrays: Part I," *Microwave Journal*, (May 1997): 288–293.
2. E. Brookner, "Major Advances in Phased Arrays: Part II," *Microwave Journal*, (June 1997): 84–92.
3. L. Eriksson and S. Broden, "High Performance Automotive Radar," *Microwave Journal*, (October 1996): 24–38.
4. A. Stove, "Automobile Radar," *Applied Microwave Magazine*, (Spring 1993): 102–115.
5. C. Berrou, A. Glavieux, and P. Thitimajshima, "Near Shannon Limit Error-Correcting Coding and Decoding: Turbo Codes," *IEEE Int. Conf. Comm., Conf. Record*, vol. 2 (May 1993): 1064–1070.
6. J. Budinger et al., "Direct Data Distribution from Low Earth Orbit," *IEEE Int'l. Conf. Comm.*, (June 1997): 662–673.
7. C.A. Jensen, J.D. Terry, and M. Vanderaar, "The Implications of Encoder/Modulator/Phased Array Designs for Future Broadband LEO Communications," *SPIE Proc.,* vol. 3232 (1997): 61–72.
8. S. Ohmori, S. Taira, and M. Austin, J. *Comm. Res. Lab.*, vol. 38, no. 2 (1991): 217.
9. D. Collier, "Optimizing LNAs for Use in Phased Arrays," *Microwave Systems News*, (April 1990): 37–45.
10. L. Dunleavy, "GaAs MMICs Perform in Phase Shifters," *Microwaves & RF* (April 1984): 49–52.
11. J. White, *Microwave Semiconductor Engineering*, (New York: Van Nostrand Reinhold Co., 1982).
12. G. Bartolucci, F. Giannini, and E. Limiti, "On the Generalized Loaded-Line Phase Shifter," *IEEE Int'l Microwave and Optoelectronics Conf. Proc.* (1995): 554–558.
13. J. Geddes, et al., "Characteristics of 30 GHz MMIC Receivers for Satellite Feed Array Application," *GaAs IC Symposium Digest*, (1987).

14. S. Ohmori, S. Taira, and M. Austin, "Beam Scanning Error of Phased Array Antenna," *Journal of Communications Research Laboratory*," vol. 38, no. 2, (July 1991) 217–222.
15. Z. Wang et al., "Single-Chip 4 Bit 35 GHz Phase-Shifting receiver with a Gb/s Digital Interface Circuitry," *GaAs IC Symposium* (1995): 234–237.
16. K. Bhasin et al., "Control of a GaAs Monolithic Ka-Band Phase Shifter Using a High-Speed Optical Interconnect," *IEEE Trans. MTT*, vol. 38, no. 5 (May 1990): 686–688.
17. S. Rossek and C. Free, "Optically Controlled Microwave Switching and Phase Shifting Using GaAs FET's," *IEEE Micro. Guided Wave Letter*, vol. 5, no.3 ((March 1995): 8–83.
18. R. Romanofsky, "On the Relationship Between Schottky Barrier Capacitance and Mixer Performance at Cryogenic Temperatures," IEEE Micro. Guided Wave Letter, vol. 6, no. 8 (August 1996): 286–288.
19. W. McLevige and V. Sokolov, "Resonated GaAs FET Devices for Microwave Switching," *IEEE Trans. Elect. Dev.*, vol. ED-28, no. 2 (February 1981): 198–204.
20. V. Sokolov, et al., "A Ka-band GaAs Monolithic Phase Shifter," *IEEE Trans. Microwave Theory Tech*, vol. MTT-31, no. 12 (December 1983): 1077–1082.
21. K. Kurokawa and W. Schlosser, "Quality Factor of Switching Diodes for Digital Modulation," *Proc. IEEE*, vol. 38 (January 1970): 180–181.
22. H. Atwater and R. Sudbury, "Use of Switching Q in the Design of FET Microwave Switches," *IEEE MTT-S Int. Microwave Symposium Digest*, (June 1981): 370–372.
23. M. Schindler and A. Morris, "DC-40 GHz and 20-40 GHz MMIC SPDT Switches," *IEEE Trans. Micro. Theory Tech*, vol. MTT-35, no. 12 (December 1987): 1486–1492.
24. 24. A. Tagantsev, "Mechanisms of Dielectric Loss in Microwave Materials," *Materials Research Society Proceedings,* 603, (2000): 221–232.
25. R. Katiyar, et al., "Investigations on Sol-Gel Derived $Ba_{0.5}Sr_{0.5}Ti_{1-\delta}Mn_{\delta}O_3$ Thin Films for Phase Shifter Applications," *Materials Research Society Proc*eedings, vol. 720 (2002): 3–14.
26. H. Wu and F. Barnes, "Doped $Ba_{0.6}Sr_{0.4}TiO_3$ Thin Films for Microwave Device Applications at Room Temperature," *Integrated Ferroelectrics*, vol. 22 (1998): 291–305.
27. N. Navi, J. Horowitz, H. Wu, and S. Qadi, "Structure-Property Relationships in W Doped (Ba,Sr)TiO3 Thin Films Deposited by Pulsed Laser Deposition on (001) MgO," *Materials Research Society Proceedings*, vol. 720 (2002); 41–48.
28. V. Varadan et al., "Ceramic Phase Shifters for Electronically Steerable Antenna Systems," *Microwave Journal*, (January 1992): 116–127.
29. V. Varadan et al., "A Novel Microwave Planar Phase Shifter," *Microwave Journal*, (April 1995): 244–253.
30. F. DeFlaviis, N. Alexopoulos, and O. Stafsudd, "Planar Microwave Integrated Phase Shifter Design with High Purity Ferroelectric Material," *IEEE Trans. MTT*, vol. 45, no. 6 (June 1997): 963–969.
31. O. Vendik, I. Mironenko, and L. Ter-Martirosyan, "Superconductors Spur Applications of Ferroelectric Films," *Microwaves & RF*, (July 1994): 67–70.
32. J. Rao, D. Patel, and L. Sengupta, "Phased Array Antennas Based on Bulk Phase Shifting with Ferroelectrics," *Integrated Ferroelectrics*, vol. 18 (1998).
33. F. Van Keuls, et al., "$YBa_2Cu_3O_{7-\delta}$, Au/SrTiO_3/LaAlO_3 Thin Film Conductor/Ferroelectric Coupled Microstripline Phase Shifters for Phased Array Applications," Applied Physics Letter, vol. 71 (November 1997): 3075–3077.
34. F. Van Keuls, et al., "Ku-Band Gold/ $Ba_xSr_{1-}xTiO_3/LaAlO_3$ Conductor/Thin Film Ferroelectric Microstripline Phase Shifter for Room Temperature Operation," *Microwave and Optical Tech. Letter*, vol. 20 (January 1999): 53–56.
35. R. Romanofsky, "Advances in Scanning Reflectarray Antennas Based on Thin Ferroelectric Film Phase Shifters," *Proc. IEEE, Special Issue on Technical Advances in Deep Space Communications and Tracking, to be published* (2007).
36. R. Romanofsky et al., "K-band Phased Array Antennas Based on $Ba_{0.60}Sr_{0.40}TiO_3$ Thin-Film Phase Shifters," *IEEE Trans. MTT*, vol. 48, no. 12 (December 2000): 2504–2510.

37. R. Romanofsky, "Broadband, Low-Loss K- and Ka-Band Phase Shifters Based on Thin Ferroelectric Films," *IEEE MTT Symposium Workshop WMC* (June 2004).
38. R. Romanofsky and A. Qureshi, "A Model for Ferroelectric Phase Shifters," *IEEE Trans. Mag.*, vol. 36, no. 5 (September 2000): 3491–3494.
39. G. M. Rebeiz, *RF MEMS Theory, Design, and Technology*, (New York: John Wiley & Sons Inc., 2003).
40. B. Lakshminarayanan and T. Weller, "Design and Modeling of 4-bit Slow-Wave MEMS Phase Shifters," *IEEE Trans. MTT*, vol. 54, no. 1 (2006): 120–127
41. N. Barker and G. Rebeiz, "Optimization of Distributed MEMS Phase Shifters," *IEEE MTT-S Digest* (1999): 299–302.
42. N. Barker and G. Rebeiz, "Distributed MEMS True-Time Delay Phase Shifters and Wide Band Switches," *IEEE Trans. MTT*, vol. 46, no. 11 (1998): 1881–1890.
43. M. Scardelletti, G. Ponchak, N. Varaljay, "MEMS, Ka-Band Single-Pole Double-Throw (SPDT) Switch for Switched Line Phase Shifters," *IEEE International Symposium on Antennas and Propagation*, (June 2002): 2–5.
44. M. Scardelletti et al., "RF MEMS Phase Shifters and Their Application in Phased Array Antennas". *IEEE Wireless and Microwave Technology Conference*, (April 2005).
45. G. Rebeiz, G-L Tan, and J. Hayden, "RF MEMS Phase Shifters: Design and Applications," *IEEE Microwave Magazine*, (June 2002): 72–82.
46. R. Romanofsky, "Slow-Wave Phase Shifters Based on Thin Ferroelectric Films, for Reflectarray Antennas," *IEEE MTT Symposium Workshop WMG*, (June 2006): 121-137.
47. A. Nagra and R. York, "Distributed Analog Phase Shifters with Low Insertion Loss," *IEEE Trans. MTT*, vol. 47, no. 9 (September 1999): 1705–1711.
48. E. Erker, et al., "Monolithic Ka-Band Phase Shifter Using Voltage Tunable $BaSrTiO_3$ Parallel Plate Capacitors," *IEEE Microwave and Guided Wave Letter*, vol. 10, no. 1 (January 2000): 10–12.
49. B. Acikel et al., "A New High Performance Phase Shifter Using $Ba_xSr_{1-x}TiO_3$ Thin Films," *IEEE Microwave and Wireless Comp. Letter*, vol. 12, no. 7 (July 2002): 237–239.
50. R. York, "BST Technology for RF Front Ends," *MTT Symposium Workshop WMG* (June 2006): 73–91.
51. G. Ponchak, "RF Transmission Lines on Silicon Substrates," 29th *European Microwave Conference*, (October 1999): 158–161.
52. G. F. Dionne et al., "Superconductivity for Improved Ferrite Devices," *Lincoln Laboratory Journal,* vol. 9, no. 1 (1996): 19–31.
53. W. Hord, "Microwave and Millimeter-Wave Ferrite Phase Shifters," *Microwave Journal, State of the Art Reference*, (1989): 81–94.
54. T. Nelson, et al., Small Analog Stripline X-Band Ferrite Phase Shifter," *IEEE Trans. MTT Correspondence*, (January 1970): 45–46.
55. D. Oates, et al., "Superconductor Ferrite Phase Shifters and Circulators," *Proc. Appl. Superconductivity Conf.*, (1996).
56. G. Dionne et al., "Ferrite-Superconductor Microwave Phase Shifters," *IEEE Trans. Mag.*, vol. 30, no. 6 (November 1994): 4518–4520.
57. D. Durand et al., "The Distributed Josephson Inductance Phase Shifter," *IEEE Trans. Appl. Superconductivity*, vol. 2, no. 1 (March1992): 33–38.
58. E. Track et al., "Investigation of an Electronically Tuned 100 GHz Superconducting Phase Shifter," *IEEE Trans. Mag.*, vol. 27, no. 2 (March 1991): 2700–2703.
59. Bednorz, J. and K. Muller, "Possible high Tc superconductivity in the Ba-La-Cu-O system," *Z. fur Phys.*, 64 (1986): 189.
60. Z-Y Shen, *High-Temperature Superconducting Microwave Circuits*, (Norwood, MA: 1994).
61. J. Martens et al., "A Reflective Switch Made of Tl-Ca-Ba-Cu-O for Signal Control Applications," *IEEE Microwave and Guided Wave Letter*, vol. 1, no. 10 (1991): 291–293.

62. Y. Tzeng et al., "High Temperature Superconductor Opening Switch," *Applied Physics Letter*, vol. 54, no. 10 (1989): 949–950.
63. W. Donaldson et al., "Interaction of Picosecond Optical Pulses with High-Tc Superconducting Films," Applied Physics Letter, vol. 54, no. 24 (1989): 2470–2472.
64. C. Jackson et al. "A High Temperature Superconductor Phase Shifter," *Microwave Journal* (December 1992): 72–78.
65. P. Mason and R. Gould, "Slow-Wave Structures Utilizing Superconducting Thin-Film Transmission Lines," *J. Appl. Phys.*, vol. 40, no. 5 (April 1969): 2039–2051.
66. F. Xiong and R. Romanofsky, "Study of Behavior of Digital Modulations for Beam Steerable Reflectarray Antennas," *IEEE Trans. Ant. and Prop.*, vol. 53, no. 3 (March 2005): 1083–1096.
67. O.S. Sands, "Beam-Switch Transient effects in the RF Path of the ICAPA Receive Phased Array Antenna," *NASA Technical Memorandum TM—2003-212588* (February 2002).
68. R. Reinhart, et al., "Phased Array Antenna-Based System Degradation at Wide Scan Angles," *IEEE International Symposium on Phased Array Systems and Technology, Revolutionary Developments in Phased Arrays* (October 2003).
69. S. K. Koul and B. Bhat, *Microwave and Millimeter Wave Phase Shifters: Vol. II Semiconductor and Delay Line Phase Shifters*, (Boston: Artech House, 1991).
70. A. Kozyrev et al., Response Time and Power Handling Capability of Tunable Microwave Devices Using Ferroelectric Films," *Integrated Ferroelectrics*, vol. 22 (1998).
71. M. Hines, "Fundamental Limitations in RF Switching and Phase Shifting Using Semiconductor Diodes," *Proc. IEEE* (June 1964): 697–708.
72. J. White, "Review of Semiconductor Microwave Phase Shifters," *Proc. IEEE*, vol. 56, no. 11, (November 1968): 1924–1930.

REPORT DOCUMENTATION PAGE

1. REPORT DATE *(DD-MM-YYYY)* 01-10-2007	2. REPORT TYPE Technical Memorandum	3. DATES COVERED *(From - To)*

4. TITLE AND SUBTITLE
Array Phase Shifters: Theory and Technology

5a. CONTRACT NUMBER

5b. GRANT NUMBER

5c. PROGRAM ELEMENT NUMBER

6. AUTHOR(S)
Romanofsky, Robert, R.

5d. PROJECT NUMBER

5e. TASK NUMBER

5f. WORK UNIT NUMBER
WBS 439432.04.04.01

7. PERFORMING ORGANIZATION NAME(S) AND ADDRESS(ES)
National Aeronautics and Space Administration
John H. Glenn Research Center at Lewis Field
Cleveland, Ohio 44135-3191

8. PERFORMING ORGANIZATION REPORT NUMBER
E-16067

9. SPONSORING/MONITORING AGENCY NAME(S) AND ADDRESS(ES)
National Aeronautics and Space Administration
Washington, DC 20546-0001

10. SPONSORING/MONITORS ACRONYM(S)
NASA

11. SPONSORING/MONITORING REPORT NUMBER
NASA/TM-2007-214906

12. DISTRIBUTION/AVAILABILITY STATEMENT
Unclassified-Unlimited
Subject Category: 32
Available electronically at http://gltrs.grc.nasa.gov
This publication is available from the NASA Center for AeroSpace Information, 301-621-0390

13. SUPPLEMENTARY NOTES
Prepared and submitted as Chapter 21: Array Phase Shifters: Theory and Technology, Antenna Engineering Handbook, McGraw Hill.

14. ABSTRACT
While there are a myriad of applications for microwave phase shifters in instrumentation and metrology, power combining, amplifier linearization, and so on, the most prevalent use is in scanning phased-array antennas. And while this market continues to be dominated by military radar and tracking platforms, many commercial applications have emerged in the past decade or so. These new and potential applications span low-Earth-orbit (LEO) communications satellite constellations and collision warning radar, an aspect of the Intelligent Vehicle Highway System or Automated Highway System. In any case, the phase shifters represent a considerable portion of the overall antenna cost, with some estimates approaching 40 percent for receive arrays. Ferrite phase shifters continue to be the workhorse in military-phased arrays, and while there have been advances in thin film ferrite devices, the review of this device technology in the previous edition of this book is still highly relevant. This chapter will focus on three types of phase shifters that have matured in the past decade: GaAs MESFET monolithic microwave integrated circuit (MMIC), micro-electromechanical systems (MEMS), and thin film ferroelectric-based devices. A brief review of some novel devices including thin film ferrite phase shifters and superconducting switches for phase shifter applications will be provided. Finally, the effects of modulo 2π phase shift limitations, phase errors, and transient response on bit error rate degradation will be considered.

15. SUBJECT TERMS
Antenna; Phase shifter circuits

16. SECURITY CLASSIFICATION OF:			17. LIMITATION OF ABSTRACT	18. NUMBER OF PAGES	19a. NAME OF RESPONSIBLE PERSON STI Help Desk (email:help@sti.nasa.gov)
a. REPORT U	b. ABSTRACT U	c. THIS PAGE U	UU	30	19b. TELEPHONE NUMBER *(include area code)* 301-621-0390